Regional Impacts of the Westerly Winds on Southern Ocean Mode and Intermediate Water Subduction

STEPHANIE M. DOWNES

Antarctic Climate and Ecosystems Cooperative Research Centre, University of Tasmania, Hobart, Tasmania, Australia

CLOTHILDE LANGLAIS

Oceans and Atmosphere, CSIRO Climate and Science Centre, Hobart, Tasmania, Australia

JORDAN P. BROOK

University of Queensland, Brisbane, Queensland, Australia

PAUL SPENCE

Centre of Excellence for Climate System Science, University of New South Wales, Sydney, New South Wales, Australia

(Manuscript received 29 May 2017, in final form 17 August 2017)

ABSTRACT

Subduction processes in the Southern Ocean transfer oxygen, heat, and anthropogenic carbon into the ocean interior. The future response of upper-ocean subduction, in the Subantarctic Mode Water (SAMW) and Antarctic Intermediate Water (AAIW) classes, is dependent on the evolution of the combined surface buoyancy forcing and overlying westerly wind stress. Here, the recently observed pattern of a poleward intensification of the westerly winds is divided into its shift and increase components. SAMW and AAIW formation occurs in regional ''hot spots'' in deep mixed layer zones, primarily in the southeast Indian and Pacific. It is found that the mixed layer depth responds differently to wind stress perturbations across these regional formation zones. An increase only in the westerly winds in the Indian sector steepens isopycnals and increases the local circulation, driving deeper mixed layers and increased subduction. Conversely, in the same region, a poleward shift and poleward intensification of the westerly winds reduces heat loss and increases freshwater input, thus decreasing the mixed layer depth and consequently the associated SAMW and AAIW subduction. In the Pacific sector, all wind stress perturbations lead to increases in heat loss and decreases in freshwater input, resulting in a net increase in SAMW and AAIW subduction. Overall, the poleward shift in the westerly wind stress dominates the SAMW subduction changes, rather than the increase in wind stress. The net decrease in SAMW subduction across all basins would likely decrease anthropogenic carbon sequestration; however, the net AAIW subduction changes across the Southern Ocean are overall minor.

1. Introduction

The Southern Ocean is a carbon distribution hub. Its overturning circulation plays a critical role in sustaining the uptake of anthropogenic carbon (Ito et al. 2010; Sallée et al. 2012; Iudicone et al. 2016). Natural carbon-rich, deep-water masses are transported southward and upwelled in the Southern Ocean, while equatorward-flowing ventilated water masses transport anthropogenic carbon toward the midlatitude region. The uptake of anthropogenic carbon is efficient in the Southern Ocean because the upwelled waters are constantly transported away from the uptake zone through Ekman transport (Ito et al. 2010) and are then transferred from the mixed layer to the ocean interior farther north, a process called subduction (Sallée et al. 2010; Langlais et al. 2017, manuscript submitted to *Sci. Rep.*, hereinafter L17). Subducted Subantarctic Mode Water (SAMW) and Antarctic Intermediate Water (AAIW) contain more than 50% of the anthropogenic carbon storage in the Southern Ocean (Sabine et al. 2004; Gruber et al. 2009; L17); however, they differ in their natural carbon content (Gruber et al. 2009). Eddies also

Corresponding author: Stephanie M. Downes, s.downes@utas.edu.au

DOI: 10.1175/JPO-D-17-0106.1

play a role in transporting heat and carbon poleward and act to offset surface Ekman transport (Morrison and Hogg 2013).

The major mode of atmospheric variability in the Southern Ocean, the southern annular mode (SAM), has been in a dominant positive phase in recent decades (Thompson and Solomon 2002; Marshall 2003). This positive phase is associated with the increase in the westerly wind speed (~30%) and approximately 3° shift poleward in the position of its maximum since the 1950s (Swart and Fyfe 2012). A positive shift in the SAM has been projected to reduce CO_2 uptake in this region caused by both increased upwelling and outgassing of natural carbon (Lenton and Matear 2007) and change the distribution of natural carbon in the upwelled deep and subducted mode and intermediate water masses [see Fig. 13 schematic in Hauck et al. (2013)]. While the Southern Ocean carbon sink may have been steadily weakening by 0.1 Pg C yr^{-1} in the last two decades (Dufour et al. 2013; Le Quéré et al. 2007; Lovenduski et al. 2007), a recent trend reversal to a larger carbon sink may have occurred (Landschützer et al. 2015). The mechanism behind the trend and its variability is at present not well understood. Thus, we are motivated to assess the role of wind stress in changing the physical circulation of water masses associated with carbon uptake.

Coarse-resolution model studies have indicated that under future climate scenarios (Downes et al. 2009, 2010), SAMW and AAIW subduction decreases by 12%–23% by the end of the twenty-first century; however, the poleward intensification of the westerly winds alone at least doubles SAMW and AAIW subduction rates (Downes et al. 2011). This study separates the influence of the shift and the intensification of the westerlies on SAMW and AAIW subduction hot spots using a high-resolution model (section 2). We determine changes in regional mixed layer depth and SAMW and AAIW subduction rates under wind stress perturbations (section 3) and then conclude in section 4.

2. Methods

a. The MOM025 configuration

The model and wind perturbations used in this study are those described in detail in Spence et al. (2014) and Hogg et al. (2017). The ocean component is the National Oceanic and Atmospheric Association Geophysical Fluid Dynamics Laboratory Modular Ocean Model, version 5 (MOM5; Griffies 2012). The eddy-permitting ocean has a ¼° horizontal grid resolution, with 50 unevenly spaced vertical levels in a geopotential depth coordinate. The model excludes any additional eddy mixing scheme. The ocean component is coupled to a sea ice model (Winton 2000), and sea surface salinity is restored to monthly climatology on a 60-day time scale. The ocean–ice model is forced by atmospheric reanalysis fluxes of sea surface temperature, wind speed, and humidity (CORE2 NYF; Large and Yeager 2009). The atmospheric state is representative of a single year in the late-twentieth century; thus, the same seasonally varying year of forcing is applied to all simulations.

Four model runs are assessed. The control (CTL) case is spun up for 500 years before three wind sensitivity experiments are initiated for 50-yr duration. After the 500-yr model spinup period, the mixed layer depth (a major driver of the net subduction rate) in the control simulation varies by no more than 10% annually. The control westerly wind stress peaks at 51°S (0.13 N m^{-2}). The wind anomalies are applied only in the 70°–25°S latitude range and are held fixed throughout the 50-yr simulations. The wind stress anomalies emulate the recently observed and modeled wind stress intensification and poleward shift and are shown in Fig. 1a. These three perturbations are 1) a 4° poleward shift of the westerly winds (SH), 2) a 30% increase in westerly wind stress (UP), and 3) a combined 4° poleward shift and 30% intensity increase (PI). The ocean's response to wind stress changes is dramatic in the first two decades (Hogg et al. 2017), thus we only compare the anomalies using the mean of the final 30 years of the control and the three perturbation runs. The westerly wind perturbations, despite being applied uniformly around the circumpolar belt, have different regional impacts on water mass properties, dependent on the latitude of the formation regions. For example, the wind stress in the UP case increases north of ~58°S. However, in the SH and PI cases, the westerlies decrease north of 45° and 35°S, respectively, with increases south of this.

b. Subduction methods

Over an annual cycle, the mixed layer deepens in autumn and winter and shoals in spring and summer. It is during the early shoaling phase, after the mixed layer depth has reached its annual maximum (Figs. 1b,c), that water masses are irreversibly transported from the mixed layer into the ocean interior (e.g., Marshall et al. 1993; Sallée et al. 2010). Thus, we describe the annual-mean subduction rate S_{ann} in terms of the annual maximum mixed layer depth H and vertical and horizontal velocities (w and $\mathbf{U}$, respectively) following methods of Marshall et al. (1993):

$$S_{ann} = w_H + \mathbf{U} \cdot \nabla H. \quad (1)$$

The subduction rate is given in units of meters per year. The annual maximum mixed layer is estimated

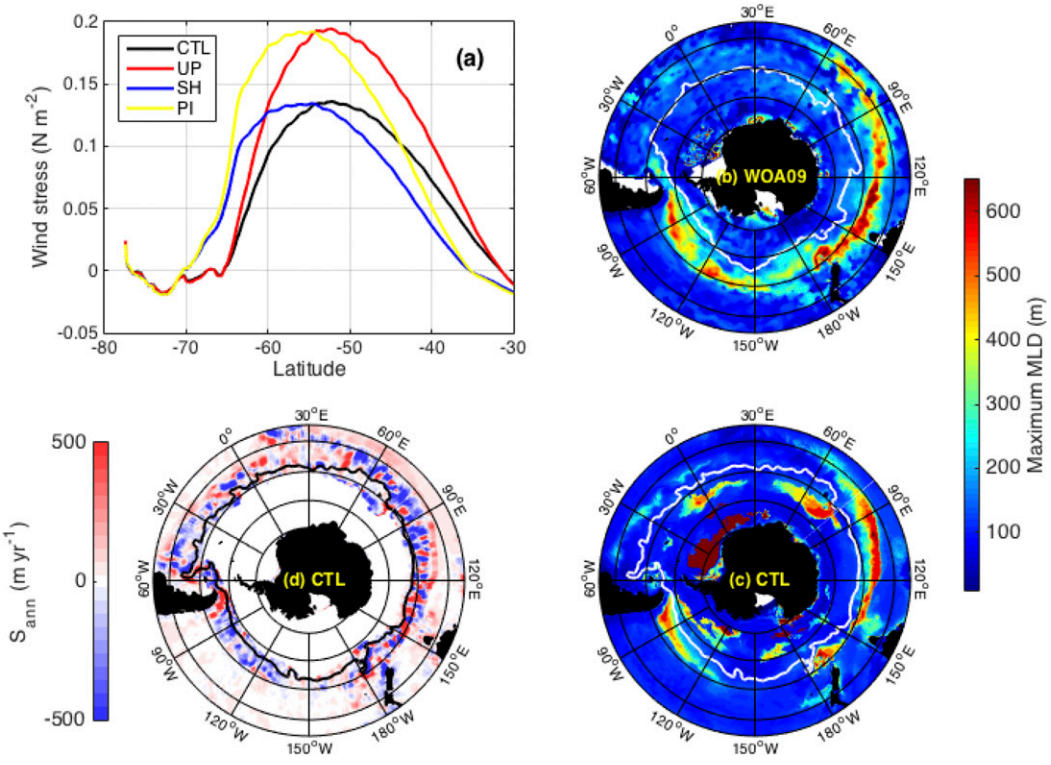

FIG. 1. (a) The zonally average zonal-mean wind stress (N m^{-2}) for the CTL (black) and three wind perturbations (increase UP, red; poleward shift SH, blue; and poleward intensification PI, yellow). The maximum monthly mixed layer depth (m) for (b) observations [*World Ocean Atlas* (*WOA09*) using a 0.03 kg m^{-3} criterion using potential density referenced to the ocean surface; Locarnini et al. 2013] and (c) the control experiment CTL (using a 0.005 kg m^{-3} criterion in potential density referenced to 2000 m). (d) The total, annual-mean subduction rate [m yr^{-1}; Eq. (1)] in the CTL experiment. Red indicates subduction into the ocean interior; blue indicates obduction (i.e., transfer from the ocean interior into the mixed layer). The analysis is limited to north of the −0.9-m mean sea surface height contour [white in (b) and (c); black in (d)].

using a 0.03 kg m^{-3} density criterion (de Boyer Montégut et al. 2004; Fig. 1b). However, the model density for high temporal resolution (required for estimating the maximum annual mixed layer depth) was only archived in the wind perturbation simulations referenced to 2000 dbar, σ_2. We have chosen a 0.005 kg m^{-3} σ_2 criterion for our study (Fig. 1c) that provides a maximum annual mixed layer comparable with 0.03 kg m^{-3} σ_0 criterion in the control run (not shown). The chosen criteria best reflect the observed magnitude of the SAMW and AAIW deep mixed layer regions in the southeast Indian and Pacific sectors, with considerably shallower mixed layers in the Atlantic (Karstensen and Tomczak 1998; Dong et al. 2008; Hartin et al. 2011). We exclude the unrealistically high mixed layers produced south of the Polar Front using the 0.005 kg m^{-3} σ_2 criterion using a −0.9-m sea surface height criterion (see contours in Fig. 1).

In the following, positive subduction is water exiting the mixed layer, and negative subduction is water entering the mixed layer (termed obduction). The SAMW and AAIW subduction rates are dominated by the lateral component (Downes et al. 2009, 2010; Sallée et al. 2010; L17). Key regions (hot spots) where subduction into the ocean interior is evident include the southeast Pacific and flowing east of Drake Passage and the southeast Indian sector (70°E–170°W; Fig. 1d). These hot spots are in agreement with those found in SAMW and AAIW density ranges in L17 (see their Fig. 3).

Several model and observational studies have separated the mean and eddy velocities in their subduction estimates (e.g., Kwon et al. 2013; L17); however, recent studies using observations and model solutions have concluded that it is the mean flow that dominates the total subduction rate in the Southern Ocean (L17). Using a 1/10° resolution MOM-based configuration with a stronger eddy energy (cf. Stewart et al. 2017), L17 found that transient eddies contribute only ~5% of the physical subduction, and ~13% to the subduction of

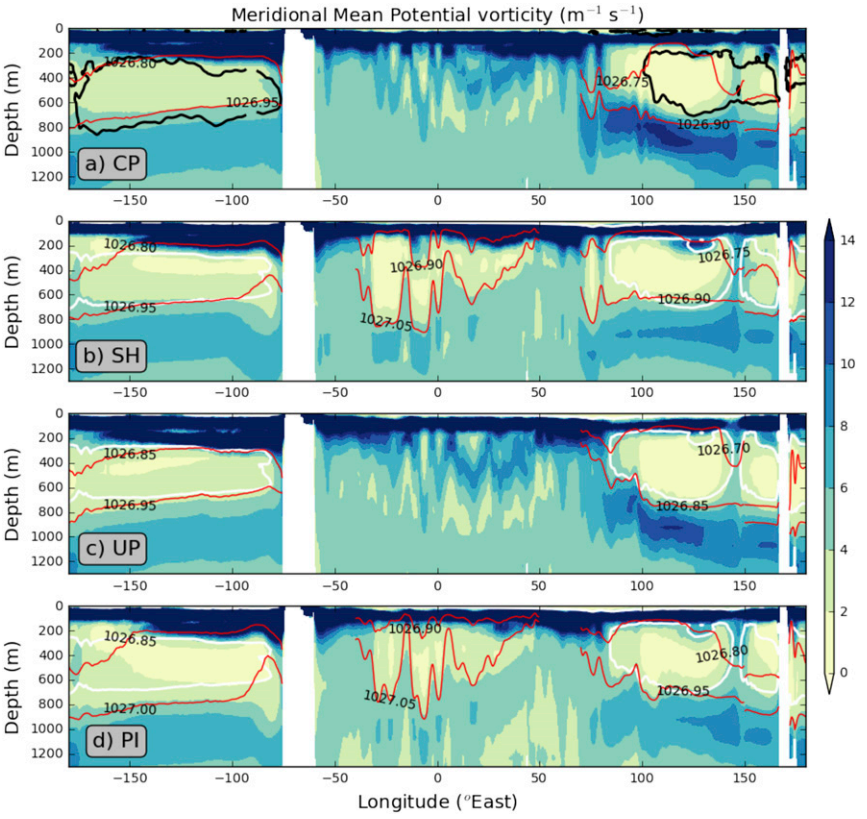

FIG. 2. Potential vorticity ($\times 10^{-11}\,\mathrm{m^{-1}\,s^{-1}}$) shown in meridional mean sections at 45°S for each experiment. Potential vorticity is defined as PV $= -(f/\rho)(\partial\rho/\partial z)$, where f is the Coriolis parameter, z is depth (positive downward), and ρ is the potential density. For comparison, the $4 \times 10^{-11}\,\mathrm{m^{-1}\,s^{-1}}$ contour line for the *WOA09* (Locarnini et al. 2013) observations is shown in the first panel (black); to be compared to the same contour level is shown from the control experiment onto each of the three wind perturbation experiments (white). The density classes bounding the PV minimum tracer for mode water in each experiment are shown in red and are tabulated for each basin in Table 1.

anthropogenic carbon, in the SAMW and AAIW density range (26.8 to 27.3 kg m^{-3}). Thus, in this study we exclude the role of eddies and solely focus on the regional changes in the mean subduction component.

3. Results

a. Water mass properties

We characterize SAMW using a low potential vorticity (PV) signature (McCartney 1977). The SAMW potential vorticity minimum lies within 1026.7 and 1026.95 kg m^{-3} (Fig. 2a), approximately 0.05 kg m^{-3} denser than observations (Table 1). The density classes vary slightly in each basin, steered by the latitudinal position of fronts and the temperature–salinity properties in each basins (Dong et al. 2008; Herraiz-Borreguero and Rintoul 2011; Hartin et al. 2011). We found that the position and density classes of SAMW in the Indian Basin change minimally under all three wind stress perturbations (Figs. 2b–d). The increase and poleward intensification wind stress perturbations both enhance local mixing and turbulence and deepen the SAMW low potential vorticity signature in the Pacific basin (Figs. 2c, d). Interestingly, the poleward shift in the Atlantic sector (SH and PI cases) dramatically shifts the upper bound of SAMW from 1026.6 to 1029.90 kg m^{-3} (Table 1). In the SH and PI cases, we find the potential vorticity minimum is not only present at 40°S as in the control (figure not shown) but also farther south at 45°S (Figs. 2b,d).

AAIW is identified by a salinity minimum (~34.4–34.6) and once subducted flows at ~700 to 1400 m (Hartin et al. 2011). Here, we use the lower SAMW density limit as the upper bound for AAIW and chose a density limit that includes the salinity minimum. The model salinity minimum tongue is thinner and does not extend as far north compared to observations, and thus the density class ranges for AAIW are smaller (cf. the observations

TABLE 1. The 30-yr mean density classes of SAMW and AAIW estimated from the annual-mean potential vorticity and salinity in each oceanic basin in the Southern Ocean. Observations are sourced from the World Ocean Atlas climatology (Locarnini et al. 2013). Basins shown are the Indian (30°–150°E), Pacific (150°E–50°W), and Atlantic (50°W–30°E).

Experiment	Region	Water mass	Density class (kg m^{-3})
Observations	Indian	SAMW	1026.65–1026.80
		AAIW	1026.80–1027.45
	Pacific	SAMW	1026.75–1026.90
		AAIW	1026.90–1027.45
	Atlantic	SAMW	1026.60–1026.80
		AAIW	1026.80–1027.45
CTL	Indian	SAMW	1026.70–1026.95
		AAIW	1026.95–1027.35
	Pacific	SAMW	1026.80–1026.95
		AAIW	1026.95–1027.40
	Atlantic	SAMW	1026.60–1026.90
		AAIW	1026.90–1027.35
SH	Indian	SAMW	1026.75–1026.95
		AAIW	1026.95–1027.40
	Pacific	SAMW	1026.80–1026.95
		AAIW	1026.95–1027.45
	Atlantic	SAMW	1026.90–1027.05
		AAIW	1027.05–1027.45
UP	Indian	SAMW	1026.70–1026.95
		AAIW	1026.95–1027.40
	Pacific	SAMW	1026.85–1026.95
		AAIW	1026.95–1027.45
	Atlantic	SAMW	1026.70–1026.95
		AAIW	1026.95–1027.40
PI	Indian	SAMW	1026.80–1026.95
		AAIW	1026.95–1027.45
	Pacific	SAMW	1026.85–1027.00
		AAIW	1027.00–1027.50
	Atlantic	SAMW	1026.90–1027.05
		AAIW	1027.05–1027.40

and CTL rows for AAIW in Table 1). In all three perturbation experiments, the AAIW density class densifies by 0.05–0.15 kg m^{-3}. An increase in the westerlies deepens the zonal-mean AAIW salinity minimum tongue (50°–35°S), while the poleward shift in the wind stress results in a southward shift of the salinity tongue (figure not shown). Despite the deepening and densification of the AAIW salinity minimum tongue, little change in the salinity of the tongue is found. Small changes in salinity may be due to the surface salinity restoring in the model or may imply that increasing and/or shifting of the westerly winds drives cooler waters from farther south into the AAIW formation regions, thus increasing the density of AAIW.

b. *Spatial patterns of variability*

The westerly wind stress is able to change the deep mixed layer regions by varying turbulence and change the temperature and salinity properties via redistribution of surface heat and freshwater forcing. We find that both the increase and poleward shift in the westerly winds steepen isopycnals south of the wind stress maximum and densify the subducted water masses, in particular AAIW (Table 1). The steepening and equatorward shift in isopycnals implies eddies are unable to fully counteract the momentum changes imparted by the wind stress perturbations.

Frankcombe et al. (2013) showed that all three wind perturbations increased the zonal transport south of the wind stress maximum, which would increase the lateral subduction of SAMW and AAIW. However, we do not find a net increase in SAMW and AAIW subduction across the Southern Ocean. Rather, regionally different changes in the mixed layer depth, and consequently subduction of SAMW and AAIW (Figs. 4a–c), are a reflection of regional changes in the surface heat and freshwater fluxes (Fig. 3). Changes in the mixed layer depth are $O(\pm 150)$ m in the regions of deep winter mixed layers (Fig. 1c), which can affect the subduction rate into the ocean interior by a factor of 2 in some regions.

The control net surface heat flux differs in sign across the Southern Ocean (Fig. 3a), whereas the mid- to high latitudes are dominated by a freshwater input (positive) that is larger to the south (Fig. 3d). In all three wind stress perturbations, increases in surface heat loss and decreases in freshwater input in the Pacific SAMW/AAIW formation regions (Fig. 3) lead to an increase in mixed layer depth and subduction in the Pacific (Fig. 4). However, a poleward migration of the westerlies shifts the SAMW and AAIW water mass formation regions toward the high-latitude upwelling zones, and we find decreases in subduction in the central Pacific (i.e., more obduction).

SAMW and AAIW formation regions are located farther north in the Indian sector compared to the Pacific, and we find different outcomes in subduction in these two regions. In the Indian sector, the poleward shift and poleward intensification cases (SH and PI) lead to a large decrease in heat loss and increase in freshwater input in the SAMW and AAIW formation regions (Figs. 3c,f). These buoyancy changes are associated with a decrease in the deep winter mixed layers just north of the wind stress maximum and a decrease in the SAMW and AAIW subduction (Fig. 4). However, despite an increase in heat gain and freshwater input in the SAMW/AAIW Indian formation regions in the increased wind stress perturbation (UP; Figs. 3b,e), we find an increase in the mixed layer depth. Thus, enhanced convection, rather than surface

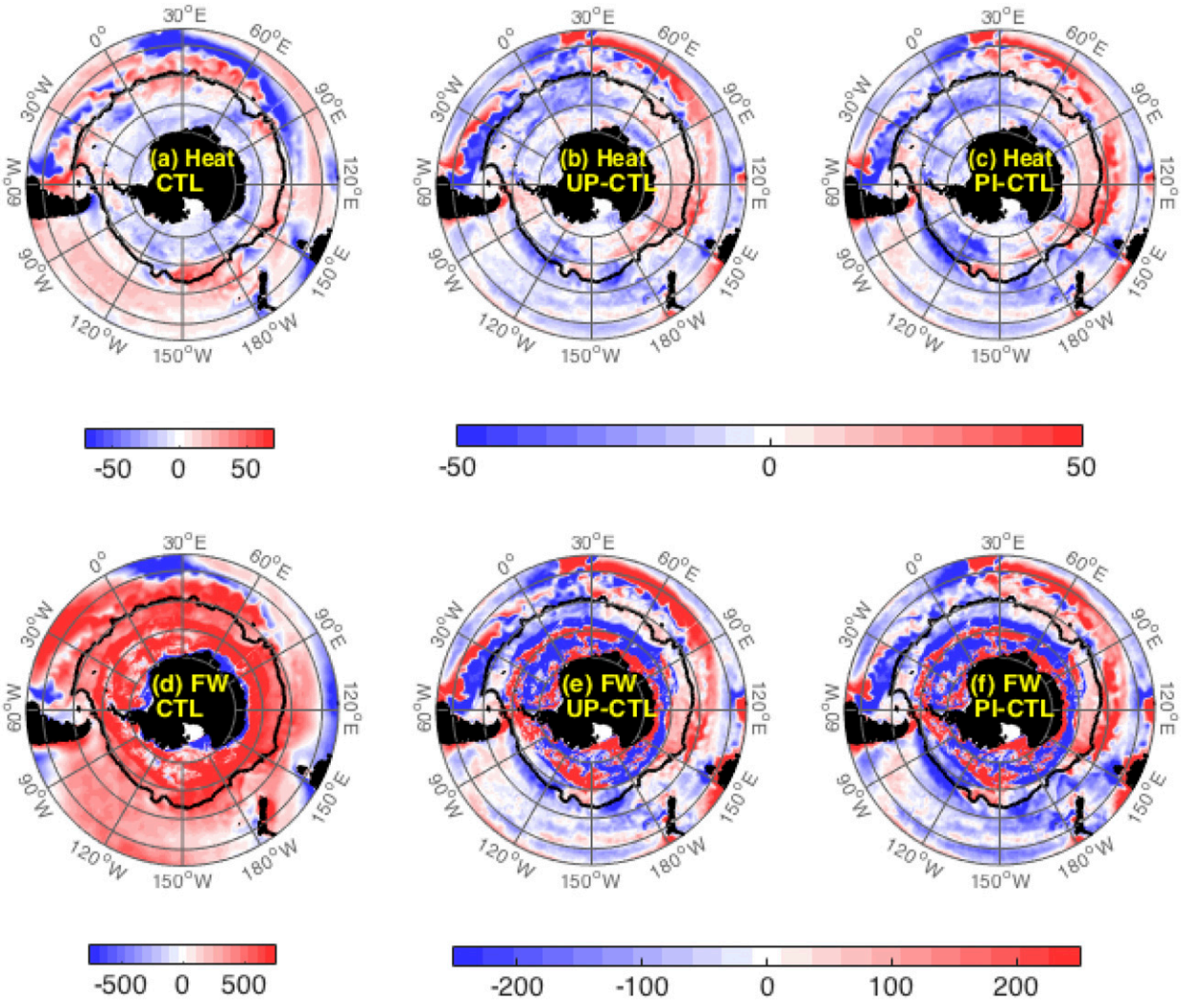

FIG. 3. (top) The net surface heat flux (positive into the ocean; $W\,m^{-2}$) for the (a) CTL, (b) UP − CTL, and (c) PI − CTL. The net surface heat flux is composed of the latent, sensible, shortwave, and longwave radiative fluxes. (bottom) As in (top), but for the net freshwater flux (positive into the ocean; $mm\,yr^{-1}$). The freshwater flux is composed of precipitation, evaporation and river runoff. The SH − CTL case is excluded as it is very similar to the PI − CTL panels. In all panels the −0.9-m sea surface height contour for the CTL case is shown in black. The analysis is limited to north of this contour.

buoyancy fluxes, more likely influences Indian SAMW and AAIW subduction in the UP experiment.

In the Atlantic basin, increased wind stress enhances surface heat loss and reduces the freshwater input (Figs. 3b,e), thus deepening the mixed layer (Fig. 4b) and increasing subduction (Fig. 4e). The region along the southern tip of South America shows distinct heat loss and freshwater input in the control case (Figs. 3a,d). Here, in both the poleward shift and poleward intensification wind stress perturbations, heat loss is reduced and the freshwater input is enhanced (Figs. 3c,f), thus shoaling the local mixed layer depth (Figs. 4a,c) and decreasing subduction (Figs. 4d,f). Directly to the west and south, the mixed layers increase because of increases in surface heat loss (Figs. 3c, 4c).

c. *Variability of net subduction rates*

While Figs. 4d and 4f illustrate the spatial pattern of the positive subduction from the mixed layer to the ocean interior, the net regional subduction rates discussed herein are a combination of the subduction and obduction processes. The net regional rates are integrated over each grid cell area and separated into $0.1\,kg\,m^{-3}$ density bins, resulting in a transport in units of Sverdrups (Sv; $1\,Sv \equiv 10^6\,m^3\,s^{-1}$; Fig. 5). In the control case, 9 Sv of SAMW is subducted in the ocean

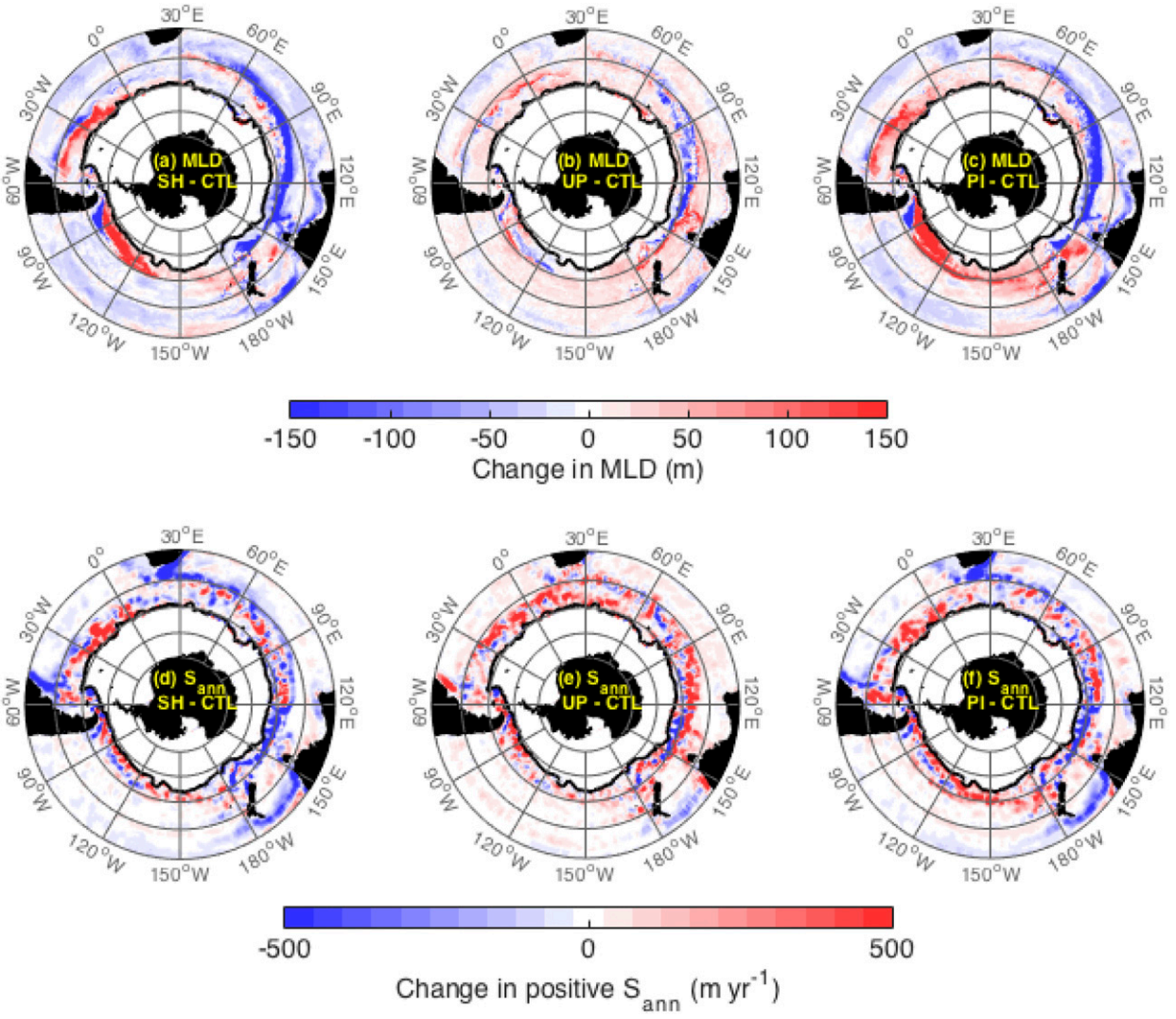

FIG. 4. The change in maximum mixed layer depth (m) from the control for each wind perturbation experiments: (a) SH − CTL, (b) UP − CTL, and (c) PI − CTL. (d)–(f) As in (a)–(c), but for the change in the positive subduction into the ocean interior ($m\,yr^{-1}$). Positive values indicate an increase in subduction; negative values a decrease in subduction. In all panels the −0.9-m sea surface height contour for the CTL case is shown in black as a reference.

interior, agreeing well with the 7 Sv diagnosed using climatology and autonomous float data (Sallée et al. 2010). In the denser AAIW layer, we find negligible transports in all regions except the central (obduction) and eastern (subduction) Pacific, which amount to 7.6 Sv subduction. Our Pacific subduction agrees favorably with the 5.8 Sv diagnosed using hydrographic chlorofluorocarbon (CFC) data by Hartin et al. (2011).

In Fig. 5, the SAMW and AAIW subduction around the circumpolar belt is divided into and summed in six uneven zonal regions for the control and three wind stress perturbations. The largest change in the SAMW formation region is the significant shoaling of the mixed layer in the southeast Indian Basin (Fig. 4), where the subduction decreases dramatically by 75% in the poleward shift and poleward intensification (SH and PI) perturbations (Fig. 5a). Conversely, the increased mixed layer depth in the northern half of the deep southeast Indian mixed layer zone (Fig. 4b) drives a small increase in the SAMW subduction in the perturbation where winds are solely increased (Fig. 5a). Obduction in the central Pacific region also increases (~50%) in the poleward shift wind stress perturbation.

The difference between the SAMW and AAIW responses to the wind perturbations is that the poleward shift in the wind stress (SH) dominates the SAMW

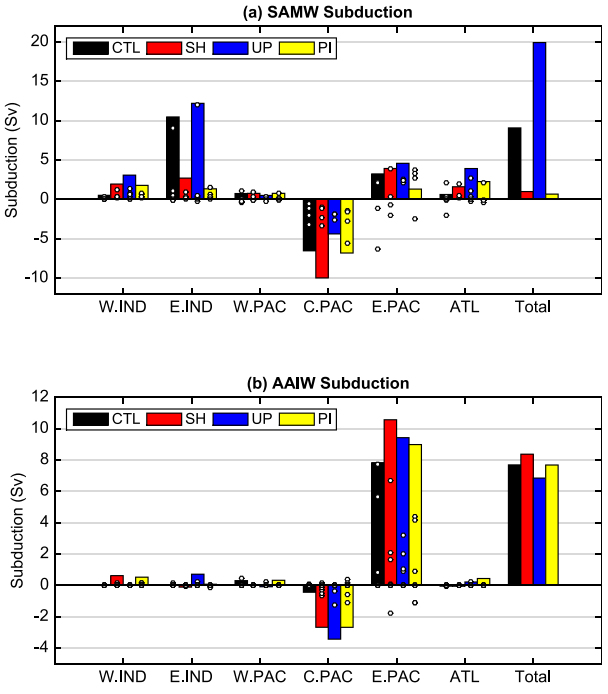

FIG. 5. Regional subduction (Sv) summed over the density classes defined in Table 1 for (a) SAMW and (b) AAIW. Shown are the CTL case (black) and three wind perturbations (increase UP, red; poleward shift SH, blue; and poleward intensification PI, yellow). The individual regions illustrated are west Indian (W.IND; 20°–90°E), east Indian (E.IND; 20°–90°E), west Pacific (W.PAC; 150°E–150°W), central Pacific (C.PAC; 150°–90°W), east Pacific (E.PAC; 90°–50°W), and Atlantic (ATL; 50°W–20°E). The total of the six regions is shown on the far right of the bottom two panels. Positive values refer to transfer from the mixed layer into the permanent thermocline. The white dots represent the subduction/obduction transports in 0.1 kg m^{-3} bins that sum to give the respective bars.

response, whereas the increase and poleward shift wind stress perturbations change similarly in the AAIW layer. The central Pacific changes in all three cases are similarly large in the AAIW layer (Fig. 5b), where obduction increases by 5 times the control rate of 0.5 Sv. Subduction in the far southeast Pacific around Drake Passage increases by up to 25%; however, the total subduction transport in this region is a combination of both significant subduction and obduction.

This study differs from that of Downes et al. (2011), where the ocean was coupled to an evolving atmosphere during a single poleward intensification experiment. While Downes et al. (2011) found an increase in SAMW and AAIW subduction under a larger poleward intensification of the westerlies, our study finds an overall decrease. This is possibly due to their larger increase in the wind stress magnitude compared with this study or the lack of coupling between the ocean and atmosphere here. Our subduction transports can also be influenced by the chosen density class for each water mass and the mixed layer density criterion; both of which can vary the subduction transports by $\sim\pm2$ Sv. However, here the dominance of the shift contribution to the impacts in the PI case persists regardless of mixed layer criterion or water mass definition.

4. Summary and conclusions

Subduction processes ventilate the ocean, allowing it to "breathe" and exchange heat, freshwater, carbon, and other gases at the air–sea interface. Here, we uniquely separate the impacts of the shift and the increase in the westerly winds on the subduction of SAMW and AAIW. We hold the atmospheric forcing quasi constant (climatology normal-year forcing) and perturb solely the winds. Water mass properties are strongly influenced by wind stress perturbations, particularly in the Atlantic sector, where a shift in the westerlies significantly expands the low potential vorticity signature of SAMW poleward. A coherent result across the Southern Ocean is that the influence of the poleward intensification of the westerly winds is dominated by its poleward shift rather than the increase in wind stress. Surface buoyancy fluxes are a major driver in regional mixed layer depth anomalies.

The strength of the overturning circulation is the critical parameter explaining the variability of carbon uptake variability in the Southern Ocean (Lenton and Matear 2007; Landschützer et al. 2015; DeVries et al. 2017). However, it is uncertain whether increased overturning circulation will cause less carbon sequestration because of upwelling of carbon-rich deep water (Le Quéré et al. 2007; Lovenduski et al. 2007; Lenton and Matear 2007) or if more carbon sequestration will occur because of enhanced subduction north of the ACC (Hauck et al. 2013). Our study adds a caveat to this view, as the poleward intensification of the winds does not result in increased SAMW and AAIW subduction. In our case, reduced subduction of anthropogenic carbon in SAMW and AAIW would reinforce the effect of upwelling of carbon-rich deep water and further limit carbon uptake. Mechanisms and feedbacks that should be considered in future work include atmospheric teleconnections as possible drivers of reduced carbon uptake (e.g., Landschützer et al. 2015) and the possibility that circulation changes could trigger a cascade of physical (e.g., Boning et al. 2008; Haumann et al. 2014) and biological feedbacks (Hauck et al. 2013).

Acknowledgments. The authors thank S. Rintoul for discussion of water mass classes and mixed layer

depths and V. Pellichero for mixed layer depth observations, particularly around the Antarctic coastline. SMD and JPB were supported by the Australian Government's Business Cooperative Research Centres Program through the Antarctic Climate and Ecosystems Cooperative Research Centre (ACE CRC). CL was supported by the CSIRO Office of Chief Executive postdoctoral fellowship. PS was supported by an Australian Research Council DECRA Fellowship DE150100223.

REFERENCES

Boning, C. W., A. Dispert, M. Visbeck, S. R. Rintoul, and F. U. Schwarzkopf, 2008: The response of the Antarctic Circumpolar Current to recent climate change. *Nat. Geosci.*, **1**, 864–869, doi:10.1038/ngeo362.

de Boyer Montégut, C., G. Madec, A. S. Fischer, A. Lazar, and D. Iudicone, 2004: Mixed layer depth over the global ocean: An examination of profile data and a profile-based climatology. *J. Geophys. Res.*, **109**, C12003, doi:10.1029/2004JC002378.

DeVries, T., M. Holzer, and F. Primeau, 2017: Recent increase in oceanic carbon uptake driven by weaker upper-ocean overturning. *Nature*, **542**, 215–218, doi:10.1038/nature21068.

Dong, S., J. Sprintall, S. T. Gille, and L. Talley, 2008: Southern Ocean mixed-layer depth from Argo profiles. *J. Geophys. Res.*, **113**, C06013, doi:10.1029/2006JC004051.

Downes, S. M., N. L. Bindoff, and S. R. Rintoul, 2009: Impacts of climate change on the subduction of mode and intermediate water masses in the Southern Ocean. *J. Climate*, **22**, 3289–3302, doi:10.1175/2008JCLI2653.1.

——, ——, and ——, 2010: Changes in the subduction of Southern Ocean water masses at the end of the twenty-first century in eight IPCC models. *J. Climate*, **23**, 6526–6541, doi:10.1175/2010JCLI3620.1.

——, A. S. Budnick, J. L. Sarmiento, and R. Farneti, 2011: Impacts of wind stress on the Antarctic Circumpolar Current fronts and associated subduction. *Geophys. Res. Lett.*, **38**, L11605, doi:10.1029/2011GL047668.

Dufour, C. O., J. L. Sommer, M. Gehlen, J. C. Orr, J.-M. Molines, J. Simeon, and B. Barnier, 2013: Eddy compensation and controls of the enhanced sea-to-air CO_2 flux during positive phases of the southern annular mode. *Global Biogeochem. Cycles*, **27**, 950–961, doi:10.1002/gbc.20090.

Frankcombe, L. M., P. Spence, A. M. Hogg, M. H. England, and S. M. Griffies, 2013: Sea level changes forced by Southern Ocean winds. *Geophys. Res. Lett.*, **40**, 5710–5715, doi:10.1002/2013GL058104.

Griffies, S. M., 2012: Elements of the Modular Ocean Model (2012 release with updates). GFDL Ocean Group Tech. Rep. 7, 618 pp.

Gruber, N., and Coauthors, 2009: Oceanic sources, sinks, and transport of atmospheric CO_2. *Global Biogeochem. Cycles*, **23**, GB1005, doi:10.1029/2008GB003349.

Hartin, C. A., R. A. Fine, B. M. Sloyan, L. D. Talley, T. K. Chereskin, and J. Happell, 2011: Formation rates of Subantarctic Mode Water and Antarctic Intermediate Water within the South Pacific. *Deep-Sea Res. I*, **58**, 524–534, doi:10.1016/j.dsr.2011.02.010.

Hauck, J., C. Völker, T. Wang, M. Hoppema, M. Losch, and D. A. Wolf-Gladrow, 2013: Seasonally different carbon flux changes in the Southern Ocean in response to the southern annular mode. *Global Biogeochem. Cycles*, **27**, 1236–1245, doi:10.1002/2013GB004600.

Haumann, F. A., D. Notz, and H. Schmidt, 2014: Anthropogenic influence on recent circulation-driven Antarctic sea ice changes. *Geophys. Res. Lett.*, **41**, 8429–8437, doi:10.1002/2014GL061659.

Herraiz-Borreguero, L., and S. R. Rintoul, 2011: Subantarctic mode water: Distribution and circulation. *Ocean Dyn.*, **61**, 103–126, doi:10.1007/s10236-010-0352-9.

Hogg, A. M., P. Spence, O. A. Saenko, and S. M. Downes, 2017: The energetics of Southern Ocean upwelling. *J. Phys. Oceanogr.*, **47**, 135–153, doi:10.1175/JPO-D-16-0176.1.

Ito, T., M. Woloszyn, and M. Mazloff, 2010: Anthropogenic carbon dioxide transport in the Southern Ocean driven by Ekman flow. *Nature*, **463**, 80–83, doi:10.1038/nature08687.

Iudicone, D., K. B. Rodgers, Y. Plancherel, O. Aumont, T. Ito, R. M. Key, G. Madec, and M. Ishii, 2016: The formation of the ocean's anthropogenic carbon reservoir. *Sci. Rep.*, **6**, 35473, doi:10.1038/srep35473.

Karstensen, J., and M. Tomczak, 1998: Age determination of mixed water masses using CFC and oxygen data. *J. Geophys. Res.*, **103**, 18 599–18 609, doi:10.1029/98JC00889.

Kwon, E. Y., S. M. Downes, J. L. Sarmiento, R. Farneti, and C. Deutsch, 2013: Role of the seasonal cycle in the subduction rates of upper–Southern Ocean waters. *J. Phys. Oceanogr.*, **43**, 1096–1113, doi:10.1175/JPO-D-12-060.1.

Landschützer, P., and Coauthors, 2015: The reinvigoration of the Southern Ocean carbon sink. *Science*, **349**, 1221–1224, doi:10.1126/science.aab2620.

Large, W., and S. G. Yeager, 2009: The global climatology of an interannually varying air–sea flux data set. *Climate Dyn.*, **33**, 341–364, doi:10.1007/s00382-008-0441-3.

Lenton, A., and R. J. Matear, 2007: Role of the southern annular mode (SAM) in Southern Ocean CO_2 uptake. *Global Biogeochem. Cycles*, **21**, GB2016, doi:10.1029/2006GB002714.

Le Quéré, C., and Coauthors, 2007: Saturation of the Southern Ocean CO_2 sink due to recent climate change. *Science*, **316**, 1735–1738, doi:10.1126/science.1136188.

Locarnini, R. A., and Coauthors, 2013: *Temperature*. Vol. 1, *World Ocean Atlas 2013*, NOAA Atlas NESIDS 73, 40 pp.

Lovenduski, N. S., N. Gruber, S. C. Doney, and I. D. Lima, 2007: Enhanced CO_2 outgassing in the Southern Ocean from a positive phase of the southern annular mode. *Global Biogeochem. Cycles*, **21**, GB2026, doi:10.1029/2006GB002900.

Marshall, G. J., 2003: Trends in the southern annular mode from observations and reanalyses. *J. Climate*, **16**, 4134–4143, doi:10.1175/1520-0442(2003)016<4134:TITSAM>2.0.CO;2.

Marshall, J. C., A. J. G. Nurser, and R. Williams, 1993: Inferring the subduction rate and period over the North Atlantic. *J. Phys. Oceanogr.*, **23**, 1315–1329, doi:10.1175/1520-0485(1993)023<1315:ITSRAP>2.0.CO;2.

McCartney, M. S., 1977: Subantarctic Mode Water. *A Voyage of Discovery: George Deacon 70th Anniversary Volume*, M. Angel, Ed., Pergamon Press, 103–119.

Morrison, A. K., and A. M. Hogg, 2013: On the relationship between Southern Ocean overturning and ACC transport. *J. Phys. Oceanogr.*, **43**, 140–148, doi:10.1175/JPO-D-12-057.1.

Sabine, C. L., and Coauthors, 2004: The oceanic sink for anthropogenic CO_2. *Science*, **305**, 367–371, doi:10.1126/science.1097403.

Sallée, J.-B., K. Speer, S. Rintoul, and S. Wijffels, 2010: Southern Ocean thermocline ventilation. *J. Phys. Oceanogr.*, **40**, 509–529, doi:10.1175/2009JPO4291.1.

——, R. J. Matear, S. R. Rintoul, and A. Lenton, 2012: Localized subduction of anthropogenic carbon dioxide in the Southern Hemisphere oceans. *Nat. Geosci.*, **5**, 579–584, doi:10.1038/ngeo1523.

Spence, P., S. M. Griffies, M. H. England, A. M. Hogg, O. A. Saenko, and N. C. Jourdain, 2014: Rapid subsurface warming and circulation changes of Antarctic coastal waters by poleward shifting winds. *Geophys. Res. Lett.*, **41**, 4601–4610, doi:10.1002/2014GL060613.

Stewart, K. D., A. M. Hogg, S. M. Griffies, A. P. Heerdegen, M. L. Ward, P. Spence, and M. H. England, 2017: Vertical resolution of baroclinic modes in global ocean models. *Ocean Modell.*, **113**, 50–65, doi:10.1016/j.ocemod.2017.03.012.

Swart, N. C., and J. C. Fyfe, 2012: Observed and simulated changes in the Southern Hemisphere surface westerly wind-stress. *Geophys. Res. Lett.*, **39**, L16711, doi:10.1029/2012GL052810.

Thompson, D. W. J., and S. Solomon, 2002: Interpretation of recent Southern Hemisphere climate change. *Science*, **296**, 895–899, doi:10.1126/science.1069270.

Winton, M., 2000: A reformulated three-layer sea ice model. *J. Atmos. Oceanic Technol.*, **17**, 525–431, doi:10.1175/1520-0426(2000)017<0525:ARTLSI>2.0.CO;2.